Structure-based design of an urokinase-type plasminogen activator receptor–derived peptide inhibiting cell migration and lung metastasis

Maria Vincenza Carriero,[1] Immacolata Longanesi-Cattani,[1] Katia Bifulco,[1] Ornella Maglio,[3,4] Liliana Lista,[3] Antonio Barbieri,[1] Giuseppina Votta,[5] Maria Teresa Masucci,[1] Claudio Arra,[1] Renato Franco,[2] Mario De Rosa,[6] Maria Patrizia Stoppelli,[5] and Vincenzo Pavone[3]

Departments of [1]Experimental Oncology and [2]Human Pathology, National Cancer Institute of Naples; [3]Department of Chemistry, University of Naples "Federico II"; [4]IBB-National Research Council; [5]Institute of Genetics and Biophysics "Adriano Buzzati-Traverso," National Research Council; and [6]Department of Experimental Medicine, Second University of Naples, Naples, Italy

Abstract

The urokinase-type plasminogen activator receptor (uPAR) plays a central role in sustaining the malignant phenotype and promoting tumor metastasis. The Ser^{88}-Arg-Ser-Arg-Tyr^{92} is the minimum chemotactic sequence of uPAR required to induce the same intracellular signaling as its ligand uPA. Here, we describe the generation of new peptide inhibitors of cell migration and invasion derived from SRSRY by a drug design approach. Ac-Arg-Glu-Arg-Phe-NH_2 (i.e., RERF), which adopts a turned structure in solution, was selected for its ability to potently prevent SRSRY-directed cell migration. Fluorescein-RERF associates with very high affinity to RBL-2H3 rat basophilic leukemia cells expressing the human formyl peptide receptor (FPR). Accordingly, femtomolar concentrations of RERF prevent agonist-dependent internalization of FPR and inhibit *N*-formyl-Met-Leu-Phe–dependent migration in a dose-dependent manner. In the absence of FPR, fluorescein-RERF binds to cell surface at picomolar concentrations in an αv integrin–dependent manner. The involvement of vitronectin receptor is further supported by the findings that 100 pmol/L RERF selectively inhibits vitronectin-dependent RBL-2H3 cell migration and prevents SRSRY-triggered uPAR/αv association. Furthermore, RERF reduces the speed of wound closure and the extent of Matrigel invasion by human fibrosarcoma HT1080 cells without affecting cell proliferation. Finally, a 3- to 5-fold reduction of lung metastasis number and size in nude mice following i.v. injection of green fluorescent protein–expressing HT1080 cells in the presence of 3.32 mg/kg RERF is observed. Our findings indicate that RERF effectively prevents malignant cell invasion *in vivo* with no signs of toxicity and may represent a promising prototype drug for anticancer therapy. [Mol Cancer Ther 2009;8(9):2708–17]

Introduction

Consolidated evidence assigns a critical role to the urokinase-type plasminogen activator receptor (uPAR) in cancer cell growth, survival, invasion, and metastasis (1–5). The uPAR potentiates cancer invasion and metastasis by focusing uPA-directed plasminogen activation to cell surface and by promoting cell survival and migration (1, 6). *In vivo*, inhibition of uPAR function or expression reduces tumor metastases, suggesting that this receptor may be regarded as a new molecular target for anticancer therapy (3, 7). Several approaches have been designed to disrupt uPAR interaction with uPA or integrins (8–10).

uPAR is a three-domain (D1, D2, and D3) protein linked to the cell surface through a COOH-terminal glycosylphosphatidylinositol anchor (11). Signaling occurs through the assembly of uPAR in composite regulatory units with transmembrane receptors, such as the formyl peptide receptor (FPR) and FPRL-1 G protein–coupled receptors, integrins, and the epidermal growth factor receptor (1, 2, 12–16). *In vivo* cleavage of the glycosylphosphatidylinositol anchor yields a soluble form of uPAR, whose amount is significantly elevated in plasma from cancer patients (11, 17).

Soluble uPAR crystal structure provides insights into receptor flexibility that enables its interaction with a variety of ligands by its external surface (18–20). Receptor engagement with uPA favors the exposure of the chemotactic Ser^{88}-Arg-Ser-Arg-Tyr^{92} sequence included in a flexible linker connecting D1 and D2 domains (21, 22). Remarkably, SRSRY synthetic peptide retains the chemotactic properties of uPAR (14). SRSRY binds to the FPR and FPRL-1 G protein–coupled receptors (12–14) and specifically promotes cytoskeletal rearrangements and directional cell migration (13). However, the conformation of SRSRY sequence in the uPA-unengaged uPAR and the

Received 2/25/09; revised 6/22/09; accepted 6/25/09; published OnlineFirst 8/25/09.

Grant support: Italian Ministry of Health grant FSN2007.

The costs of publication of this article were defrayed in part by the payment of page charges. This article must therefore be hereby marked *advertisement* in accordance with 18 U.S.C. Section 1734 solely to indicate this fact.

Note: Supplementary material for this article is available at Molecular Cancer Therapeutics Online (http://mct.aacrjournals.org/).

Requests for reprints: Maria Vincenza Carriero, Department of Experimental Oncology, National Cancer Institute of Naples, Via M. Semmola, 80131 Naples, Italy. Phone: 39-815903569; Fax: 39-815903814. E-mail: mariolinacarriero@yahoo.it

doi:10.1158/1535-7163.MCT-09-0174

conformational preferences of the SRSRY peptide are still unexplored. Recently, we developed synthetic peptides carrying specific amino acid substitutions along the SRSRY sequence and found that the Arg-Glu-Arg central core is relevant to the inhibition of the SRSRY-dependent cell migration (23). Among the pentapeptides, pyroGlu-Arg-Glu-Arg-Tyr-NH_2 (pERERY-NH_2) was found to inhibit cell migration in culture (23). To investigate the structural requirements for this inhibitory effect, we analyzed the conformation of the peptides Arg-X_1-Arg-X_2 (X_1 = Ser, Glu; X_2 = Tyr, Phe, Trp) using the Protein Data Bank (PDB) as a large ensemble of structures that may significantly represent the energy allowable conformations for a given amino acid sequence (24). By this approach, we have designed the Ac-Arg-Glu-Arg-Phe-NH_2 tetrapeptide (i.e., RERF), which has a high propensity to adopt a turned structure in solution and inhibits SRSRY-dependent cell migration at a 500× to 1,000× lower concentration than pERERY-NH_2. The novel peptide blocks FPR activity and αv-dependent cell migration at femtomolar concentrations. Remarkably, RERF prevents human fibrosarcoma HT1080 cell invasion in a mouse model of lung colonization, suggesting the development of RERF-based compounds as new anticancer agents.

Materials and Methods

Peptide Synthesis and Purification

Peptides, synthesized by the solid-phase approach using standard Fmoc methodology in a manual reaction vessel, were purified by RP-HPLC-C18 column to a 99% purity (25). Fluoresceinated RERF (FITC-RERF) was synthesized by the on-resin procedure using ε-aminocaproic acid as spacer. It retains the 97% of the inhibitory activity on cell migration. Molecular weights were confirmed by mass spectrometry.

Cell Cultures

Human embryonic kidney HEK-293 and HEK-293/uPAR cells (26), rat basophilic leukemia RBL-2H3 and RBL-2H3/ETFR cells (27), and human fibrosarcoma HT1080 cells were grown in DMEM-10% fetal bovine serum (FBS). Silencing of αv expression was done on 1×10^6 RBL-2H3 cells transfected either with control small interfering RNA (siRNA) or with 60 nmol/L 5′-CCAUAUGGUGGCGAAGAUA-3′ siRNA, a 19-nucleotide sequence corresponding to nucleotides 1393 to 1412 of αv (Sigma-Aldrich) as previously described (26), using HiPerFect transfection reagent (Qiagen). Transfectants were analyzed 48 h later. HT1080 transfectants stably expressing the green fluorescent protein (GFP) were obtained using pEGFP-N1 vector (Clontech) and FuGene6 transfection reagent (Roche). Twenty G418-resistant clones were screened by a fluorescence inverted microscope and by Western blot using anti-GFP polyclonal antibody (BD Biosciences). Clone 19 expressing the highest levels of GFP was chosen for further studies.

Migration and Invasion Assays

Chemotaxis assays were done in Boyden chambers using 8-μm pore size filters at 37°C, 5% CO_2 (13). Briefly, 1×10^5 viable cells suspended in serum-free DMEM were allowed to migrate for 4 h toward DMEM containing the indicated effectors. For invasion assays, filters were coated with 70 μg/mL Matrigel (BD Biosciences), and 3×10^4 cells per chamber were allowed to migrate toward DMEM-10% FBS with or without the indicated peptides for 18 h (28). At the end of both assays, cells on the lower filter surface were fixed and stained with hematoxylin and 10 random fields per filter were counted at ×200 magnification.

Coimmunoprecipitation of αv/uPAR Complexes

HEK-293/uPAR cells were lysed in radioimmunoprecipitation assay buffer and 400 μg/sample were incubated overnight at 4°C with 5 μg/mL VNR147 anti-αv monoclonal antibody (mAb; Chemicon) as described (13, 26). Proteins copurified with αv were recovered by protein G-Sepharose and analyzed by a 10% SDS-PAGE followed by Western blot with 2 μg/mL R4 anti-uPAR mAb or 1 μg/mL anti-αv antibody (Chemicon).

Association of Biotinylated D288-183 uPAR to Cell Surface

Recombinant D288-183 (5 μg; Calbiochem) was biotinylated using the Amersham kit (GE Healthcare). Cells were exposed to 100 nmol/L biotin-D288-183 in DMEM-1% bovine serum albumin for 2 h at 4°C, and surface-associated proteins were recovered by acidic treatment (29).

Fluorescence Microscopy

Cytoskeleton was analyzed on suspended HEK-293 cells, as previously described (13). For the *N*-formyl-Met-Leu-Phe (fMLF) internalization experiments, cells were grown adherent on glass slides, incubated with the indicated effectors for 30 min at 37°C, and then exposed to 10 nmol/L *N*-formyl-Nle-Leu-Phe-Nle-Tyr-Lys-fluorescein (Molecular Probes) for additional 30 min at 37°C (30). Cells were visualized using a Zeiss 510META-LSM microscope, and z-series with 0.5-μm intervals were collected.

Binding Assays

Cells grown adherent on glass slides were incubated with the indicated effectors or anti–vitronectin receptor (VnR) antibodies (5 μg/mL; Chemicon) in DMEM-1 mg/mL bovine serum albumin for 60 min at 4°C and then exposed to FITC-RERF for 60 min at 4°C. Cells transfected with siRNAs were analyzed in suspension for binding to FITC-RERF or anti-VnR antibodies for 60 min at 4°C. Quantitative image analysis was done using a LMS510 Zeiss confocal microscope on 100 cells per sample with the Axiovision 4.4 software (Carl Zeiss). Hill's equation (31) for two independent binding sites is $y = (100 + a \cdot x / kd1) / (1 + x / kd1) + (a + b \cdot x / kd2) / (1 + x / kd2) - a$, where $kd1$ and $kd2$ are the apparent dissociation constants, a is the value of y at saturation of the first site, and b is the value of y at saturation of the second site. Hill's slope was fixed to 1. Hill's equation for one binding site is $[100 + a\ (x / kd)^b] / [1 + (x / kd)^b]$, where kd is the apparent dissociation constant, a is the value of y at saturation, and Hill's slope (b) was 0.24. Experimental points were fitted to the above equations by using a standard least-square procedure.

Wound-Healing Assay

Confluent HT1080 cells in a 24-multiwell plate were wounded with a sterile pipette tip and exposed to 10% FBS-DMEM with or without 100 pmol/L RERF. Plates were kept at 37°C in a 5% CO_2 of a Zeiss inverted microscope equipped with a motorized stage. One field that includes the scratched path from each dish was selected and scanned sequentially every 15 min for 20 h.

Proliferation Assay

HT1080 cells (1.5×10^3 per well) were grown in 96-multiwell flat-bottomed plates in 10% FBS-DMEM in the presence of 10 μmol/L RERF or diluents. At the indicated times, suspended cells were removed and the adherent cells were stained with MTT dye (Sigma-Aldrich) for 4 h at 37°C as described (32).

Lung Colonization Model

Twenty 6- to 8-wk-old CD1 female nude mice of 23 to 25 g were maintained in a germ-free environment. Housing and handling of mice were in accordance with institutional guidelines complying with national and international laws and policies. All mice received an injection of GFP-tagged HT1080 as a single-cell suspension (2.5×10^6 cells in 100 μL of sterile PBS, 97% viability) in the tail vein. After 24 h, the animals were randomized into two groups. Ten animals received every 48 h i.v. injections of 100 μL PBS containing 3.32 mg/kg RERF per mouse and 10 animals received injections of 100 μL PBS. After 22 d, mice were weighted and sacrificed by cervical dislocation. Lungs were removed, sectioned, and fixed in buffered 4% formaldehyde and examined blindly. The number of lung metastases was assessed in three H&E-stained sections per mouse and expressed as mean metastases number/mm^2. The extent of normal and tumor lung parenchyma was measured in three fields per sample on H&E-stained sections. Area of lung metastasis was assessed using the Axiovision 4.4 software. Right lower lobe from each lung was lysed as described (15), and 50 μg proteins/sample were analyzed by Western blot using 1 μg/mL anti-GFP antibody or 1 μg/mL anti–α-tubulin mAb (Sigma-Aldrich). Densitometry was done by NIH Image 1.62 software (Bethesda, MD). For histologic and GFP expression data, statistical analysis was done using the Student's *t* test. Differences were considered statistically significant if $P < 0.05$.

Results

Conformational Preferences of the Arg-X_1-Arg-X_2 Sequence

To investigate the conformational preferences of the Arg-X_1-Arg-X_2 sequence (X_1: any amino acid; X_2: Tyr, Phe, Trp), we searched in the PDB (24) for the most frequently observed conformations of the sequence Arg-X_1-Arg-X_2. The database included 406 protein structures (Supplementary Data) solved by X-ray crystallography, at a resolution of 2.8 Å or better, and with a sequence identity cutoff up to 50%. In the case of proteins having multiple chains with the same sequence, only one chain was considered. α-Turns are defined as reported in reference (33). β-Extended and β-turn conformation are defined as previously reported (34). According to Ramakrishnan and Nataraj (35), 42.3% of the structures are α-turned, 42.4% are β-extended, and 15.3% are irregular (mixed β-extended and β-turned; ref. 34).

Fig. 1A shows the percentage of Arg-X_1-Arg-X_2 sequences with α-turned or β-extended conformation for each amino acid at the X_1 position. Ser is present in 26 structures with an about equal distribution among the three different classes of conformations. This suggests that Arg-Ser-Arg-Tyr could be accommodated either in an α-turned or β-extended conformation. Instead, Glu is observed 26 times (of 33 cases) in an α-turn conformation (78.6%, quite above the average value of 42.3%) followed by Lys and Gln. Trp, Pro, and Val are mainly observed in the β-extended conformation. Cys is observed in α-turn conformation in two of three structures only. These findings allowed us to conclude that the Arg-Glu-Arg-X_2 sequence might be the best candidate to obtain a compact turned structure. Figure 1B and C depicts the superposition of the β-extended (Fig. 1B) and α-turned (Fig. 1C) structures of Arg-Ser-Arg-Tyr sequences as found in the PDB. Figure 1D depicts the superposition of the α-turned structure in Arg-Glu-Arg-Tyr sequences. The α-turned structure has the following characteristics: an aromatic residue is spatially flanked by two basic residues (Arg), and a Glu residue is opposite to the aromatic residue. Overall, these theoretical findings prompted us to examine the biological properties of RERX_2 peptides (X_2: Tyr, Phe, Trp). Furthermore, to avoid the perturbing effects of the end charges on the conformational preferences, we synthesized NH_2-terminal acetylated and COOH-terminal amidated RERW, RERY, and RERF peptides.

Effects of RERW, RERY, and RERF on SRSRY-Directed Cell Migration

The effects on cell migration of RERW, RERY, and RERF were evaluated by conventional Boyden chamber assays using HEK-293 cells, which do not express uPAR and respond to SRSRY motogen stimulus (13). Unlike RERY, RERW and RERF at 1 μmol/L concentration significantly reduced basal cell migration, although to a different extent (75% and 57% of the random cell migration, respectively). In combination with 10 nmol/L SRSRY, equimolar concentrations of RERW, RERY, and RERF reduced SRSRY-dependent cell migration by 59%, 49%, and 45%, respectively, whereas the control peptide ARARY was ineffective. RERF exerted the strongest inhibition and was further characterized for its conformational preferences and biological activity.

Nuclear Magnetic Resonance Structure of RERF

We investigated the conformational preferences of RERF in water and in water/trifluoroethanol by circular dichroism and nuclear magnetic resonance spectroscopy (RERF conformational preferences; Supplementary Tables S1 and S2; Supplementary Figs. S1–S3). RERF, although displaying some conformational flexibility, preferentially adopts an α-turn (type I-α_{RS}; ref. 35) in both solvent systems (Fig. 1E). This conformation is similar to that observed for the α-turned structures found in our subset of the PDB (compare Fig. 1E with Fig. 1C and D).

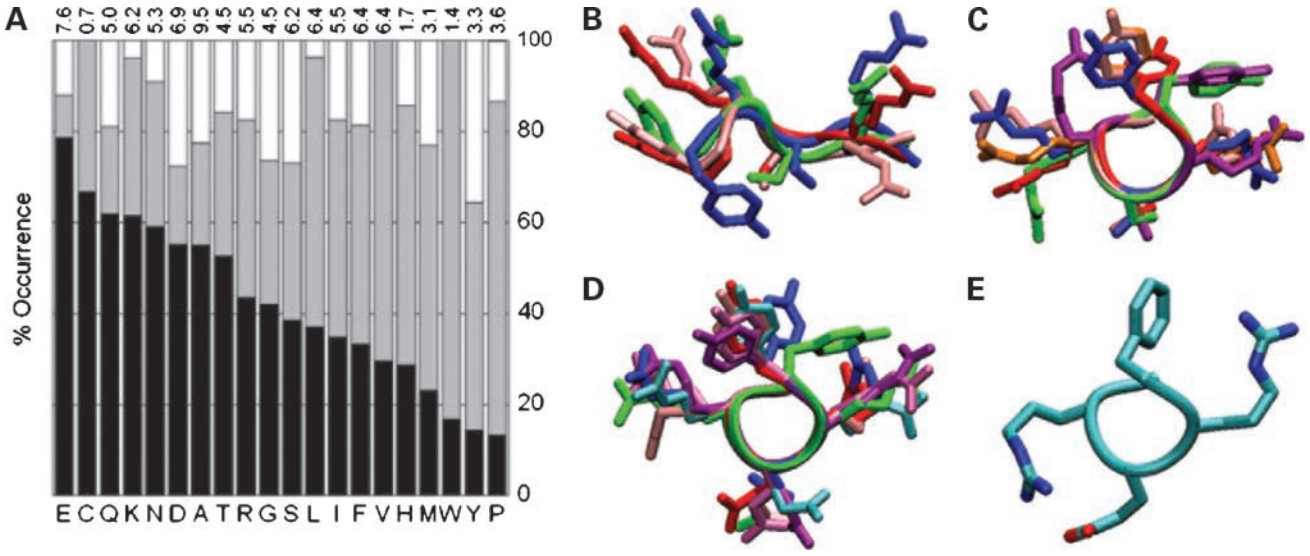

Figure 1. Structural analysis. **A,** analysis of the conformational preferences of Arg-X_1-Arg-X_2 sequences (X_1 = any amino acid, X_2 = Phe, Tyr, Trp) as found in our subset of the PDB. *Columns,* percentage of occurrence of α-turned (*black columns*), β-extended (*gray columns*), and all the other structures (*white columns*) for each amino acid (*single-letter codes*) at the X_1 position. The occurrence of each amino acid at the X_1 position is also indicated on the top as percentage of the total. **B** to **D,** superposition of the Cα atoms of the Arg-X-Arg-Tyr sequence (found in our subset of the PDB). **B,** X = Ser in β-extended conformation. The depicted proteins (PDB codes) are 1BGN (*blue*), 1ZDZ (*red*), 1VKD (*green*), and 1SKZ (*pink*). **C,** X = Ser in α-turn conformation. The depicted proteins are 1FCH (*blue*), 1I6A (*red*), 1JJ8 (*orange*), 1LVA (*green*), 1QSA (*pink*), and 1UMZ (*purple*). **D,** X = Glu in α-turn conformation. The depicted proteins are 2BL9 (*mauve*), 1Z2U (*purple*), 1Y96 (*cyan*), 1SAZ (*pink*), 1LI4 (*green*), 1EM8 (*red*), and 1BWV (*blue*). **E,** average molecular conformation of RERF as derived from nuclear magnetic resonance analysis in water/trifluoroethanol solution.

RERF Is an Antagonist of SRSRY Activity

Our previous work allowed the identification of the peptide pERERY-NH_2, inhibiting cell migration in culture (23). Both RERF and pERERY-NH_2 inhibited SRSRY-induced HEK-293 cell migration in a dose-dependent manner (Fig. 2A). Remarkably, the effect of RERF starts in the attomolar concentration range, reaching an overall 75% inhibition above 10 nmol/L. In addition, the IC_{50} of RERF seems to be 500- to 1,000-fold lower compared with pERERY-NH_2. According to our previous evidence, SRSRY-treated HEK-293 cells exhibit F-actin filamentous structures localized in polarized regions (13). Although RERF alone did not affect cytoskeleton, cell preincubation with RERF prevented SRSRY-triggered actin polymerization (Fig. 2B).

To test whether RERF may prevent uPAR/VnR association and subsequent SRSRY-dependent signaling (13), RERF-treated HEK-293/uPAR cells were exposed to 10 nmol/L SRSRY and the lysates were immunoprecipitated with anti-αv antibody. The amount of uPAR copurified with αv chain was revealed by Western blot. As shown in Fig. 2C, RERF did not appreciably affect the basal uPAR/αv physical association but consistently decreased the amount of uPAR copurified with αv chain in cells exposed to SRSRY. These findings suggest that RERF may inhibit SRSRY-dependent migration and cytoskeletal rearrangements by preventing uPAR/integrin association.

High-Affinity Binding and Regulation of FPR by RERF

To identify the membrane component/s mediating the inhibitory effect of RERF, we tested whether RERF binds to the FPR, which specifically associates with SRSRY (13). HEK-293 cells were preincubated with an excess unlabeled D288-183 uPAR fragment, SRSRY, RERF, or ARARY, and then exposed to biotinylated D288-183. Acid-eluted biotinylated proteins were analyzed for the biotin content. As shown in Fig. 2D, all effectors, except ARARY, prevent cell association of biotinylated D288-183 to a similar extent, suggesting that SRSRY and RERF share the same surface binding site.

To test whether RERF binds directly to FPR, we used RBL-2H3/ETFR cells that stably express FPR (23). RBL-2H3/ETFR cells were preincubated at 4°C (to avoid internalization) with the indicated concentrations of fMLF, ARARY, or the scrambled peptide ERFR and then exposed to different concentrations of FITC-RERF at 4°C. Cell exposed to 100 fmol/L or 100 pmol/L of FITC-RERF showed a clear-cut punctuated pattern. A concentration of FITC-RERF as low as 100 fmol/L was still effective for staining cells (Fig. 3A). Decoration with 100 pmol/L FITC-RERF was strongly reduced by preincubation with fMLF but ARARY or ERFR (Fig. 3A). Remarkably, 10 fmol/L unlabeled RERF decreases cell-associated FITC-RERF by 50%, and maximal reduction is reached at 10 pmol/L unlabeled RERF (Fig. 3B). The experimental points could well be fitted (R = 0.994) with two independent binding site Hill's equation, with Kd_{app}s of $8 \pm 1.6 \times 10^{-17}$ mol/L and $2.2 \pm 2 \times 10^{-9}$ mol/L (Fig. 3B), suggesting the occurrence of two binding sites.

FPRs are internalized in response to agonist stimulation, this process being a prerequisite for receptor activation

(30, 36). We evaluated the effect of RERF on agonist-dependent FPR internalization on RBL-2H3/ETFR cells. The cells were preincubated at 37°C with fMLF, ARARY, or increasing concentration of RERF and then exposed to *N*-formyl-Nle-Leu-Phe-Nle-Tyr-Lys-fluorescein. As expected, on cell exposure to the fluorescent agonist at 37°C, FPR seemed mainly internalized as indicated by green fluorescent intracytoplasmic spots that were prevented by the use of nonfluorescent fMLF (Fig. 3C). These results were further confirmed by z-stack analysis of confocal images (Supplementary Image to Fig. 3C). Unlike ARARY, 1 fmol/L, 1 pmol/L, or 1 nmol/L of RERF prevented agonist internalization (Fig. 3C). These results indicate that RERF interferes with FPR biological activity either by inducing FPR internalization or by blocking agonist-FPR interaction.

Furthermore, migration of RBL-2H3/ETFR cells toward fMLF is strongly inhibited by RERF (Fig. 3D). Consistently with competition binding assays with FITC-RERF (Fig. 3B), inhibition by RERF starts in the attomolar range, an overall 72% inhibition being observed above 1 to 10 nmol/L RERF.

In conclusion, these experiments show that femtomolar concentrations of RERF specifically associate to an FPR-expressing cell line and inhibit fMLF-dependent FPR internalization and migration.

Involvement of VnR in the Inhibitory Activity of RERF

The possibility that two sites are involved in binding of RERF to cell surface was studied in RBL-2H3 cells lacking FPR. We reasoned that if these cells bear a low-affinity binding site for RERF, they may be stained by higher concentrations of FITC-RERF. Unlike RBL-2H3/ETFR cells, RBL-2H3 cells were unreactive to 100 amol/L or 100 fmol/L of FITC-RERF. The FPR-negative cells react only with FITC-RERF at a concentration of ≥100 pmol/L. The binding was specific as it was abrogated by unlabeled RERF but ARARY or ERFR (Fig. 4A). Competition binding assays revealed that the experimental points could well be fitted with a single site Hill's equation (Kd_{app}, $1.4 + 1 \times 10^{-13}$ mol/L; $R = 0.994$; Fig. 4B), indicating the occurrence of a high-affinity binding site for RERF in the absence of FPR.

To explore the involvement of integrins as partners of RERF, we analyzed RBL-2H3 cell migration toward the following integrin ligands: 25 μg/mL vitronectin, 100 μg/mL fibronectin, 50 μg/mL laminin, or 50 μg/mL collagen. As shown in Fig. 4C, RERF did not prevent fibronectin- or laminin-dependent cell migration and slightly reduced collagen-directed migration. On the contrary, 1 nmol/L RERF caused a 45% reduction of vitronectin-directed migration, whereas 10 fmol/L RERF was ineffective (Fig. 4C). In agreement with the competition binding assay (Fig. 4B), inhibition by FITC-RERF starts in the picomolar range and reaches maximal inhibition in the nanomolar range (Fig. 4C).

To test peptide binding to VnR, RBL-2H3 cells were incubated with 100 pmol/L FITC-RERF following preexposure to a panel of monoclonal or polyclonal antibodies recognizing αvβ3 or αvβ5 VnRs. Cell fluorescence was not reduced by blocking LM609 anti-αvβ3 or P1F6 anti-αvβ5

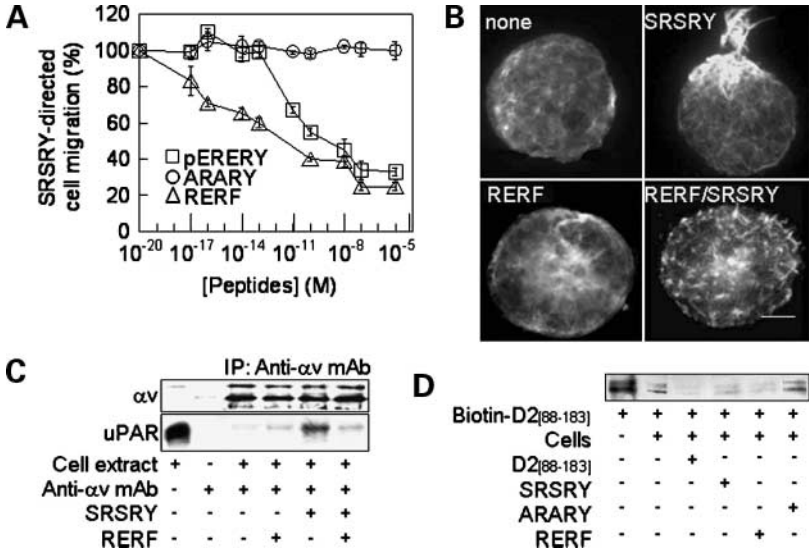

Figure 2. Effect of RERF on the functional activity of SRSRY. **A,** concentration-dependent effect of RERF on SRSRY-directed HEK-293 cell migration in Boyden chambers. Cells were allowed to migrate toward 10 nmol/L SRSRY in the presence of increasing concentrations of the indicated peptides. Values (100%) represent the extent of SRSRY-dependent cell migration in the absence of peptides. *Points,* mean of four experiments in triplicate; *bars,* SD. **B,** representative images of rhodamine-phalloidin–stained HEK-293 cells exposed to diluents (*none*) or the indicated effectors at 10 nmol/L. Original magnification, ×630. *Scale bar,* 3 μm. **C,** effect of RERF on uPAR/αv association. HEK-293/uPAR cells preincubated with 100 pmol/L RERF or diluents for 15 min were exposed to 10 nmol/L SRSRY or diluents for 45 min. Lysates (400 μg/sample) were immunoprecipitated using VNR147 anti-αv mAb and analyzed by Western blot with R4 anti-uPAR mAb or anti-αv antibody. Cell extract (10 μg) or 1 μg anti-αv mAb was loaded as controls. Similar results were obtained in three independent experiments. **D,** effect of RERF on the binding of biotin-D2[88-183] to HEK-293 cell surface. HEK-293 cells (1×10^6 per sample) incubated with 500 nmol/L D2[88-183], SRSRY, RERF, ARARY, or diluents for 15 min were exposed to biotin-D2[88-183]. Acid-eluted proteins were analyzed by Western blot. Biotin-D2[88-183] (5 μL) was loaded as a control. Similar results were obtained in two independent experiments.

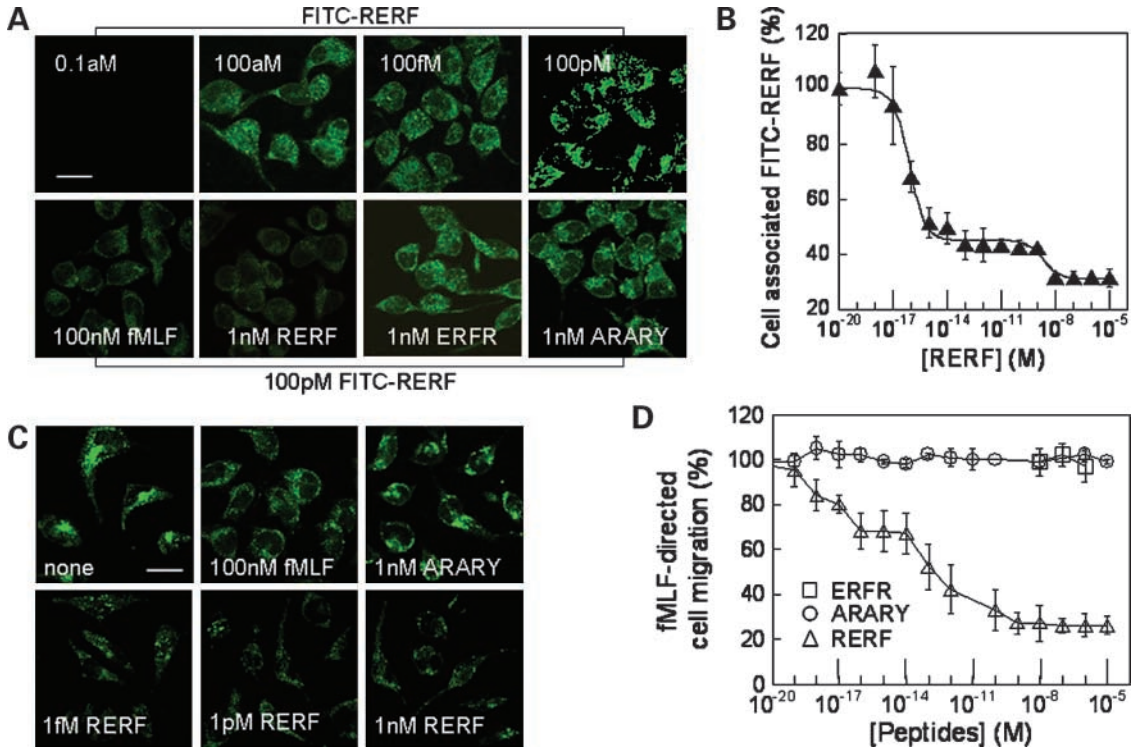

Figure 3. Involvement of FPR in the inhibitory effect of RERF. **A,** representative images of RBL-2H3/ETFR cells exposed to the indicated concentrations of FITC-RERF (*top*) at 4°C or exposed to 100 pmol/L FITC-RERF (*bottom*) with the indicated peptides at 4°C. Original magnification, ×630. *Scale bar,* 10 μm. **B,** quantification of the cell-associated fluorescence was done as described in Materials and Methods. *Points,* mean of two independent experiments done in duplicate; *bars,* SD. **C,** effect of RERF on fMLF-triggered FPR internalization. Representative confocal images of RBL-2H3/ETFR cells incubated at 37°C with diluents (*none*), or the indicated effectors, and exposed to *N*-formyl-Nle-Leu-Phe-Nle-Tyr-Lys-fluorescein. Original magnification, ×630. *Scale bar,* 10 μm. **D,** concentration-dependent effect of RERF on fMLF-directed RBL-2H3/ETFR cell migration. The extent of cell migration in the presence of increasing concentrations of RERF, ARARY, or ERFR was expressed as a percentage of the fMLF-dependent cell migration (100%). *Points,* mean of five independent experiments in duplicate; *bars,* SD.

mAb(s), suggesting that the RGD integrin recognition site is not involved. Unlike anti-αv antibody recognizing integrin cytoplasmic domain (amino acids 1022–1034), anti-VnR antibodies and P3G8 anti-αv mAb strongly reduced surface-associated fluorescence (Fig. 4D). To further test whether RERF binds to αv chain of the VnR, we reduced the αv expression in FPR lacking RBL-2H3 cells. Consequently, this silencing leads to the strong reduction of FITC-RERF binding to RBL-2H3 cells (Fig. 4D). Taken together, these findings indicate that RERF interacts with αv chain of VnR, thereby preventing vitronectin-directed cell migration.

Inhibition of HT1080 Cell Migration and Invasion by RERF

The clear-cut ability of RERF to prevent HEK-293 and RBL-2H3 cell migration prompted us to test whether this inhibition extends to highly invasive human fibrosarcoma HT1080 cells (37), expressing a considerable amount of VnR and migrating toward fMLF (15).[7] First, we tested whether RERF prevents directional HT1080 cell migration in Boyden chamber assays. As shown in Fig. 5A, migration toward 10 nmol/L fMLF or 10% FBS was inhibited by RERF but ARARY or the scrambled ERFR. In both cases, inhibition starts at ~1 fmol/L, 50% of maximal effect is reached in the femtomolar range, and 70% inhibition is observed above 10 nmol/L RERF (Fig. 5A). Then, we tested whether RERF prevents HT1080 spreading in a wound-healing assay monitored for 20 hours by time-lapse videomicroscopy (attached movie). Wounds disappeared after 18 hours in the presence of 10% FBS and the addition of 100 pmol/L RERF strongly reduced the extent of wound repair. RERF caused a 1.8-fold reduction (1.23 versus 0.67 μm/min) in the cell speed during wound closure (Fig. 5B). We also found that RERF inhibits HT1080 cell invasion in a dose-dependent manner. Inhibition starts in the femtomolar range, and it seems to level off in the nanomolar range and reaches an overall 55% reduction at 10 nmol/L (Fig. 5C).

The effects on migration and invasion are not due to a reduced proliferation rate because 10 μmol/L RERF did not modify cell growth up to 96 hours (Fig. 5D). The ability of RERF to prevent migration and invasion of malignant fibrosarcoma cells in culture suggests that it may counteract tumor spreading and metastasis *in vivo*.

[7] I. Longanesi-Cattani and M.V. Carriero, unpublished data.

Inhibitory Effect of RERF on Lung Colonization by Fibrosarcoma Cells

To study the *in vivo* effect of RERF in a mouse lung colonization model, GFP-tagged HT1080 cells (2.5×10^6) were injected in the tail vein of 20 nude mice. The day after, 10 animals received, every 48 hours for 22 days, 3.32 mg/kg RERF and 10 received injections of vehicle only. Mice weight was monitored and time-dependent average weight increase showed that the animals survived the treatment schedule without changes in body weight (Fig. 6A). In all cases, intraparenchymal and subpleural lung metastatic foci were observed (Fig. 6B). Histologic analysis showed more numerous metastases in untreated versus RERF-treated mice. The mean number of lung metastases/mm^2 in RERF-treated and untreated mice was 40.4 and 15.3, respectively, with $P < 0.001$ (Fig. 6D). Accordingly, morphometric analysis of lung metastatic foci revealed a mean neoplastic area significantly lower in RERF-treated than untreated mice (15.2% versus 42.5% of total section, respectively, with $P < 0.001$; Fig. 6D). GFP quantitative analysis revealed that GFP content was 4- to 5-fold lower in RERF-treated than untreated mice (4.6 versus 21.1 of α-tubulin content, respectively, with $P < 0.001$; Fig. 6C and D). A significant correlation between relative GFP expression levels and lung metastases areas ($P < 0.0001$) was also found (Fig. 6D). Although we cannot exclude that RERF could affect tumor growth *in vivo*, our findings indicate that RERF effectively prevents malignant cell lung colonization at low dosage. It is noteworthy that the animals do not show signs of toxicity, suggesting that RERF represents a promising prototype drug for anticancer therapy.

Discussion

By a drug design approach based on the conformational analysis of Ser^{88}-Arg-Ser-Arg-Tyr^{92} (SRSRY) chemotactic sequence of uPAR, we have developed a potent inhibitor of cell migration. The Ac-Arg-Glu-Arg-Phe-NH_2 (RERF) tetrapeptide displays a high propensity to adopt a turned structure in solution and is a potent inhibitor of *in vitro* and *in vivo* cell invasion of highly malignant human fibrosarcoma HT1080 cells.

By sequential substitution of single residues, we have previously dissected the SRSRY sequence and identified the core amino acids relevant to the motogen effect. We also generated the pentapeptide pERERY-NH_2, which inhibits migration of cultured cells at picomolar concentrations (23). Remarkably, the novel RERF peptide inhibits cell migration at a 500- to 1,000-fold lower concentration than pERERY-NH_2 ($IC_{50} \approx 2 \times 10^{-11}$ mol/L). When administered

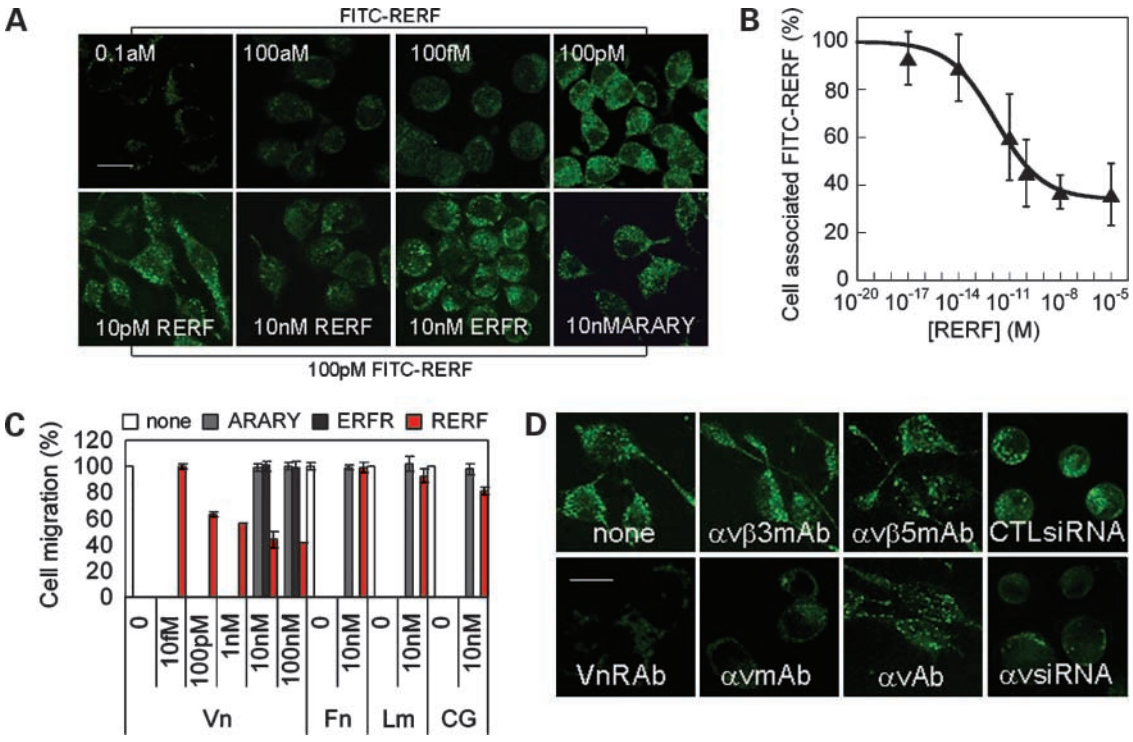

Figure 4. Involvement of VnR in the inhibitory effect of RERF. **A,** representative images of RBL-2H3 cells preincubated with diluents, or the indicated peptides, and then exposed to the indicated concentrations of FITC-RERF at 4°C. *Scale bar,* 10 μm. **B,** cell-associated fluorescence was quantified as described in Materials and Methods. *Points,* mean of two independent experiments in duplicate; *bars,* SD. **C,** chemotactic response of RBL-2H3 cells to vitronectin (*Vn*), fibronectin (*Fn*), laminin (*Lm*), or collagen (*CG*) with or without the indicated effectors. Residual cell migration was expressed as a percentage of directional migration toward the indicated chemoattractants in the absence of peptides (100%). *Columns,* mean of two independent experiments done in duplicate; *bars,* SD. **D,** representative images of RBL-2H3 cells preincubated with diluents (*none*), or the indicated antibodies, or transfected with control siRNA or with αv siRNA and then exposed to 100 pmol/L FITC-RERF. Original magnification, ×630. *Scale bar,* 10 μm.

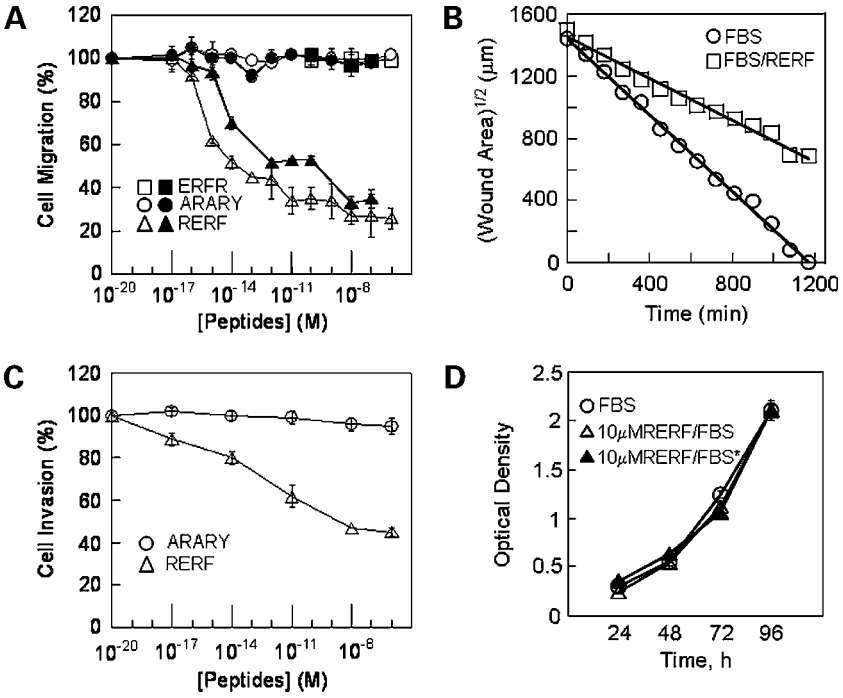

Figure 5. Effects of RERF on HT1080 cell migration, invasion, and proliferation. **A,** cell migration assays of HT1080 cells toward 10 nmol/L fMLF (*empty symbols*) or 10% FBS (*filled symbols*) combined with increasing concentration of the indicated peptides. The extent of migration is expressed as a percentage of chemoattractant-directed cell migration (100%). *Points,* mean of three experiments in duplicate; *bars,* SD. **B,** wound healing of HT1080 cells incubated with DMEM/10% FBS in the presence or absence of 100 pmol/L RERF. One field that includes the scratched path from each dish was recorded sequentially every 15 min for 20 h by a video camera connected with a motorized inverted microscope. The extent of wounded areas was evaluated by the Axiovision 4.4 software. Best-fit linear equations are $y = 1{,}439 - 1.23x$ ($R = 0.998$) and $y = 1{,}452 - 0.669x$ ($R = 0.993$) for FBS and FBS/RERF, respectively. **C,** Matrigel invasion of HT1080 cells toward 10% FBS combined with increasing concentration of RERF or ARARY. The extent of invasion is expressed as a percentage of FBS-directed cell invasion (100%). *Points,* mean of three experiments in duplicate; *bars,* SD. **D,** time-dependent proliferation of HT1080 cells in the presence of serum with or without 10 μmol/L RERF. When indicated (*), medium was replaced every 24 h. *Points,* mean of two experiments done in duplicate; *bars,* SD.

in vivo, RERF is apparently well tolerated, as weights of mice injected with vehicle or vehicle containing RERF were comparable. Furthermore, liver, spleen, and kidneys did not show any morphologic evidence of organ toxicity (data not shown). In addition, we did not notice the occurrence of adverse side effects that might hamper the therapeutic potential of RERF. In culture, RERF prevents cell migration more effectively than invasion (75% versus 55% decrease; Fig. 5C), suggesting that perhaps the enzymatic inhibition of plasminogen activators and metalloproteinases may further block *in vivo* tumor invasion (38). Our results indicate that RERF does not affect animal growth but effectively

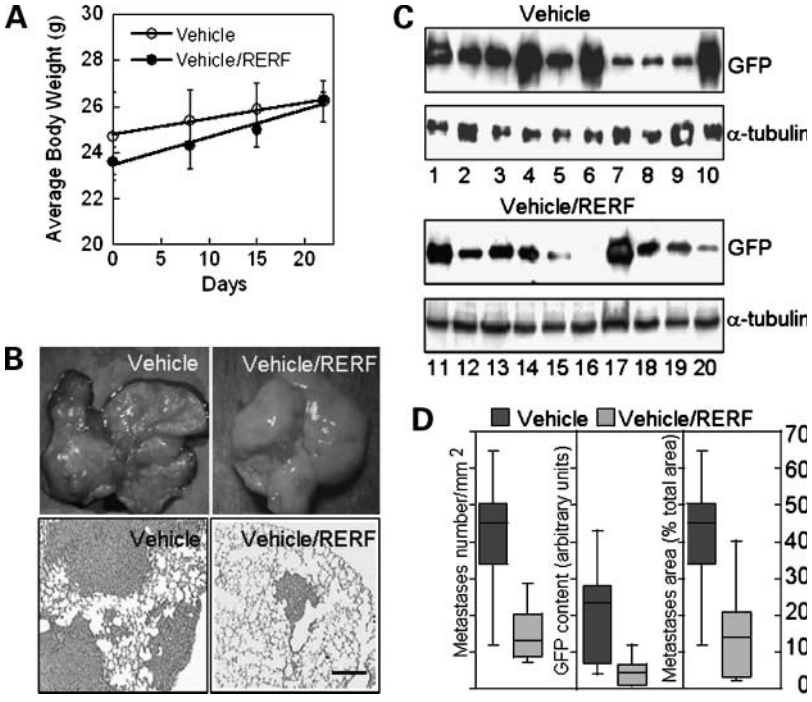

Figure 6. Inhibitory effect of RERF on mice lung colonization by HT1080 cells. GFP-tagged HT1080 cells were injected in the tail vein of 20 nude mice. Ten animals received 3.32 mg/kg RERF and 10 received injections of vehicle every 48 h for 22 d. **A,** time-dependent average increase in body weight of RERF-treated versus untreated mice. Average from the observed values is reported. **B,** macroscopic view of lungs and H&E-stained sections at ×40 magnification derived from the lung of untreated (*Vehicle*) mouse n.5 and the lung of treated (*Vehicle/RERF*) mouse n.15. *Scale bar,* 50 μm. **C,** GFP and α-tubulin content assessed on representative lung sample per mouse by Western blot. **D,** number of metastases/mm^2, relative extent of GFP expression (normalized against α-tubulin), and metastasis areas measured on H&E-stained sections at ×100 magnification of untreated (*Vehicle*) and treated (*Vehicle/RERF*) mice.

prevents tumor cell dissemination, although we cannot ascertain how RERF exactly functions. It could affect lung dissemination by inhibiting extravasation and cell adhesion or by forcing tumor cells into dormancy.

Interestingly, RERF inhibition extends from the attomolar to the nanomolar concentration range, possibly reflecting the occurrence of multiple sites. In binding experiments, RERF associates with high affinity to FPR and competes with fMLF, suggesting that they share the same site. Alternatively, as the ligand binding pocket of FPR consists of several key residues located in different transmembrane helices (39), RERF/FPR association may affect fMLF adjacent binding. Interestingly, RERF displays a higher affinity for FPR than fMLF, preventing agonist-dependent FPR internalization and migration at a concentration as low as 0.1 to 1 fmol/L.

Our data show that RERF selectively binds to the αv integrin subunit and inhibits vitronectin-dependent cell migration, whereas it does not affect collagen-, fibronectin-, and laminin-directed migration. Interestingly, αvβ5 modulates uPAR-dependent cell migration (15, 26), and its activity is regulated by the SRSRY uPAR sequence via FPR (13). Furthermore, whereas the "connecting peptide" region of uPA binds directly to αvβ5 integrin, thus conveying a motogen signaling, its phosphorylated form renders the protease an inhibitor of cell migration through αvβ5 (26, 40).

X-ray studies show the flexibility of the uPAR domain organization, suggesting that unengaged uPAR may exist in a latent form and then may be subjected to a conformational change on ligand binding (41). Our *in silico* studies suggest that the sequence Arg-Ser-Arg-Tyr could be accommodated in either an α-turned or β-extended conformation, raising the possibility that these different states may coexist in intact uPARs and regulate SRSRY chemotactic activity. According to this hypothesis, RERF would mimic the inhibitory α-turned conformation. However, these speculations need testing with the full receptor molecule. Our experimental approach holds a high potential to identify new protein-protein interactions and define important pathways in tumor invasion and metastasis. Although RERF has a high affinity and efficacy in cell culture and mouse, its therapeutic potential remains to be ascertained.

Emerging experimental and clinical data indicate that G protein–coupled receptors have a crucial role in cancer progression and metastasis (42). Among these, FPR increases the phosphorylation of the epidermal growth factor receptor intracellular receptor tail, transactivating the receptor and supporting tumor progression (43). Although FPR antagonists have been investigated mostly for their putative role as anti-inflammatory agents (44), they may be promising as anticancer agents. The combined abilities of RERF to inhibit both FPR and VnR suggest that this prototype inhibitor may prove useful in tumor targeting and anticancer therapies.

Disclosure of Potential Conflicts of Interest

No potential conflicts of interest were disclosed.

Acknowledgments

We thank G. Hoyer-Hansen (Finsen Institute, Copenhagen, Denmark) who kindly provided the R4 anti-uPAR mAb and G. Di Carluccio for the technical assistance.

References

1. Blasi F, Carmeliet P. uPAR: a versatile signaling orchestrator. Nat Rev Mol Cell Biol 2002;3:932–43.

2. Ossowski L, Aguirre-Ghiso JA. Urokinase receptor and integrin partnership: coordination of signaling for cell adhesion, migration and growth. Curr Opin Cell Biol 2000;12:613–20.

3. Jacobsen B, Ploug M. The urokinase receptor and its structural homologue C4.4A in human cancer: expression, prognosis and pharmacological inhibition. Curr Med Chem 2008;15:2559–73.

4. Alfano D, Franco P, Vocca I, et al. The urokinase plasminogen activator and its receptor: role in cell growth and apoptosis. Thromb Haemost 2005; 93:205–11.

5. Del Vecchio S, Stoppelli MP, Carriero MV, et al. Human urokinase receptor concentration in malignant and benign breast tumors by *in vitro* quantitative autoradiography: comparison with urokinase levels. Cancer Res 1993;53:3198–206.

6. Dano K, Behrendt N, Hoyer-Hansen G, et al. Plasminogen activation and cancer. Thromb Haemost 2005;93:676–81.

7. Romer J, Nielsen BS, Ploug M. The urokinase receptor as a potential target in cancer therapy. Curr Pharm Des 2004;10:2359–76.

8. Pillay V, Dass CR, Choong PF. The urokinase plasminogen activator receptor as a gene therapy target for cancer. Trends Biotechnol 2007; 25:33–9.

9. Degryse B, Resnati M, Czekay RP, Loskutoff DJ, Blasi F. Domain 2 of the urokinase receptor contains an integrin-interacting epitope with intrinsic signaling activity: generation of a new integrin inhibitor. J Biol Chem 2005;280:24792–803.

10. Sato S, Kopitz C, Schmalix WA, et al. High-affinity urokinase-derived cyclic peptides inhibiting urokinase/urokinase receptor-interaction: effects on tumor growth and spread. FEBS Lett 2002;528:212–6.

11. Rasch MG, Lund IK, Almasi CE, Hoyer-Hansen G. Intact and cleaved uPAR forms: diagnostic and prognostic value in cancer. Front Biosci 2008; 13:6752–62.

12. Montuori N, Carriero MV, Salzano S, Rossi G, Ragno P. The cleavage of the urokinase receptor regulates its multiple functions. J Biol Chem 2002;277:46932–9.

13. Gargiulo L, Longanesi-Cattani I, Bifulco K, et al. Cross-talk between fMLP and vitronectin receptors triggered by urokinase receptor-derived SRSRY peptide. J Biol Chem 2005;280:25225–32.

14. Resnati M, Pallavicini I, Wang JM, et al. The fibrinolytic receptor for urokinase activates the G protein-coupled chemotactic receptor FPRL1/LXA4R. Proc Natl Acad Sci U S A 2002;99:1359–64.

15. Carriero MV, Del Vecchio S, Capozzoli M, et al. Urokinase receptor interacts with α(v)β5 vitronectin receptor, promoting urokinase-dependent cell migration in breast cancer. Cancer Res 1999;59:5307–14.

16. Kugler MC, Wei Y, Chapman HA. Urokinase receptor and integrin interactions. Curr Pharm Des 2003;9:1565–74.

17. Sidenius N, Blasi F. The urokinase plasminogen activator system in cancer: recent advances and implication for prognosis and therapy. Cancer Metastasis Rev 2003;22:205–22.

18. Llinas P, Le Du MH, Gårdsvoll H, et al. Crystal structure of the human urokinase plasminogen activator receptor bound to an antagonist peptide. EMBO J 2005;24:1655–63.

19. Huai Q, Mazar AP, Kuo A, et al. Structure of human urokinase plasminogen activator in complex with its receptor. Science 2006; 311:656–9.

20. Barinka C, Parry G, Callahan J, et al. Structural basis of interaction between urokinase-type plasminogen activator and its receptor. J Mol Biol 2006;363:482–95.

21. Gårdsvoll H, Ploug M. Mapping of the vitronectin-binding site on the urokinase receptor: involvement of a coherent receptor interface consisting of residues from both domain I and the flanking interdomain linker region. J Biol Chem 2007;282:13561–72.

22. Huai Q, Zhou A, Lin L, et al. Crystal structures of two human

vitronectin, urokinase and urokinase receptor complexes. Nat Struct Mol Biol 2008;15:422–3.

23. Bifulco K, Longanesi-Cattani I, Gargiulo L, et al. An urokinase receptor antagonist that inhibits cell migration by blocking the formyl peptide receptor. FEBS Lett 2008;582:1141–6.

24. Berman HM, Westbrook J, Feng Z, et al. The Protein Data Bank. Nucleic Acids Res 2000;28:235–42.

25. Fields GB, Noble RL. Solid phase peptide synthesis utilizing 9-fluorenylmethoxycarbonyl amino acids. Int J Pept Protein Res 1990;35:161–214.

26. Franco P, Vocca I, Carriero MV, et al. Activation of urokinase receptor by a novel interaction between the connecting peptide region of urokinase and (α)v(β)5 integrin. J Cell Sci 2006;119:3424–34.

27. Hall AL, Wilson BS, Pfeiffer JR, Oliver JM, Sklar LA. Relationship of ligand-receptor dynamics to actin polymerization in RBL-2H3 cells transfected with the human formyl peptide receptor. J Leukoc Biol 1997;62: 535–46.

28. Silvestri I, Longanesi-Cattani I, Franco P, et al. Engaged urokinase receptors enhance tumor breast cell migration and invasion by up-regulating αvβ5 vitronectin receptor cell surface expression. Int J Cancer 2002;102:562–71.

29. Carriero MV, Del Vecchio S, Franco P, et al. Vitronectin binding to urokinase receptor in human breast cancer. Clin Cancer Res 1997;3: 1299–308.

30. Bennett TA, Maestas DC, Prossnitz ER. Arrestin binding to the G protein-coupled *N*-formyl peptide receptor is regulated by the conserved "DRY" sequence. J Biol Chem 2000;275:24590–4.

31. Weiss JN. The Hill equation revisited: uses and misuses. FASEB J 1997;11:835–41.

32. Baroni A, Donnarumma G, Paoletti I, et al. Antimicrobial human β-defensin-2 stimulates migration, proliferation and tube formation of human umbilical vein endothelial cells. Peptides 2009;30:267–72.

33. Kabsch W, Sander C. Dictionary of protein secondary structure: pattern recognition of hydrogen-bonded and geometrical features. Biopolymers 1983;22:2577–637.

34. Pavone V, Gaeta G, Lombardi A, et al. Discovering protein secondary structures: classification and description of isolated α-turns. Biopolymers 1996;38:705–21.

35. Ramakrishnan C, Nataraj DV. Energy minimization studies on α-turns. J Pept Sci 1998;4:239–52.

36. Perez DM, Karnik SS. Multiple signaling states of G-protein-coupled receptors. Pharmacol Rev 2005;57:147–61.

37. Yamamoto N, Jiang P, Yang M, et al. Cellular dynamics visualized in live cells *in vitro* and *in vivo* by differential dual-color nuclear-cytoplasmic fluorescent-protein expression. Cancer Res 2004;64:4251–6.

38. Deryugina EI, Quigley JP. Matrix metalloproteinases and tumor metastasis. Cancer Metastasis Rev 2006;25:9–34.

39. Miettinen HM, Mills JS, Gripentrog JM, Dratz EA, Granger BL, Jesaitis AJ. The ligand binding site of the formyl peptide receptor maps in the transmembrane region. J Immunol 1997;159:4045–54.

40. Vocca I, Franco P, Alfano D, et al. Inhibition of migration and invasion of carcinoma cells by urokinase-derived antagonists of αvβ5 integrin activation. Int J Cancer 2009;124:316–25.

41. Yuan C, Huang M. Does the urokinase receptor exist in a latent form? Cell Mol Life Sci 2007;64:1033–7.

42. Dorsam RT, Gutkind JS. G-protein-coupled receptors and cancer. Nat Rev Cancer 2007;7:79–94.

43. Huang J, Chen K, Gong W, et al. Receptor "hijacking" by malignant glioma cells: a tactic for tumor progression. Cancer Lett 2008;267: 254–61.

44. Yan P, Nanamori M, Sun M, et al. The immunosuppressant cyclosporin A antagonizes human formyl peptide receptor through inhibition of cognate ligand binding. J Immunol 2006;177:7050–8.